Test of Shi et al. method to infer the magnetic reconnection geometry from spacecraft data: MHD simulation with guide field and antiparallel kinetic simulation

R. E. Denton,[1] B. U. Ö. Sonnerup,[2] M. Swisdak,[3] J. Birn,[4] J. F. Drake,[3] and M. Hesse[5]

Received 27 April 2012; revised 28 June 2012; accepted 7 July 2012; published 6 September 2012.

[1] When analyzing data from an array of spacecraft (such as Cluster or MMS) crossing a site of magnetic reconnection, it is desirable to be able to accurately determine the orientation of the reconnection site. If the reconnection is quasi-two dimensional, there are three key directions, the direction of maximum inhomogeneity (the direction across the reconnection site), the direction of the reconnecting component of the magnetic field, and the direction of rough invariance (the "out of plane" direction). Using simulated spacecraft observations of magnetic reconnection in the geomagnetic tail, we extend our previous tests of the direction-finding method developed by Shi et al. (2005) and the method to determine the structure velocity relative to the spacecraft $\boldsymbol{V}_{str}$. These methods require data from four proximate spacecraft. We add artificial noise and calibration errors to the simulation fields, and then use the perturbed gradient of the magnetic field $\boldsymbol{B}$ and perturbed time derivative $d\boldsymbol{B}/dt$, as described by Denton et al. (2010). Three new simulations are examined: a weakly three-dimensional, i.e., quasi-two-dimensional, MHD simulation without a guide field, a quasi-two-dimensional MHD simulation with a guide field, and a two-dimensional full dynamics kinetic simulation with inherent noise so that the apparent minimum gradient was not exactly zero, even without added artificial errors. We also examined variations of the spacecraft trajectory for the kinetic simulation. The accuracy of the directions found varied depending on the simulation and spacecraft trajectory, but all the directions could be found within about 10° for all cases. Various aspects of the method were examined, including how to choose averaging intervals and the best intervals for determining the directions and velocity. For the kinetic simulation, we also investigated in detail how the errors in the inferred gradient directions from the unmodified Shi et al. method (using the unperturbed gradient) depended on the amplitude of the calibration errors. For an accuracy of 3° for the maximum gradient direction, the calibration errors could be as large as 3% of reconnection magnetic field, while for the same accuracy for the minimum gradient direction, the calibration errors could only be as large as 0.03% of the reconnection magnetic field. These results suggest that the maximum gradient direction can normally be determined by the unmodified Shi et al. method, while the modified method or some other method must be used to accurately determine the minimum gradient direction. The structure velocity was found with magnitude accurate to 2% and direction accurate to within 5%.

Citation: Denton, R. E., B. U. Ö. Sonnerup, M. Swisdak, J. Birn, J. F. Drake, and M. Hesse (2012), Test of Shi et al. method to infer the magnetic reconnection geometry from spacecraft data: MHD simulation with guide field and antiparallel kinetic simulation, *J. Geophys. Res.*, *117*, A09201, doi:10.1029/2012JA017877.

[1]Department of Physics and Astronomy, Dartmouth College, Hanover, New Hampshire, USA.
[2]Thayer School of Engineering, Dartmouth College, Hanover, New Hampshire, USA.
[3]Institute for Research and Electronics and Applied Physics, University of Maryland, College Park, Maryland, USA.
[4]Los Alamos National Laboratory, Los Alamos, New Mexico, USA.
[5]NASA Goddard Space Flight Center, Greenbelt, Maryland, USA.

Corresponding author: R. E. Denton, Department of Physics and Astronomy, Dartmouth College, Hanover, NH 03755, USA. (richard.e.denton@dartmouth.edu)

0148-0227/12/2012JA017877

1. Introduction

[2] One of the major goals of magnetospheric spacecraft observations is to investigate spatial structures such as sites of magnetic reconnection. The starting point for such investigations is to determine the orientation of the structure relative to the spacecraft. While there has been considerable research on methods to determine the direction across a one dimensional discontinuity from spacecraft observations [*Sonnerup et al.*, 2006, and references therein; see also *Mozer and Retinò*, 2007], there has been less research on methods to determine the orientation of two-dimensional structures. In

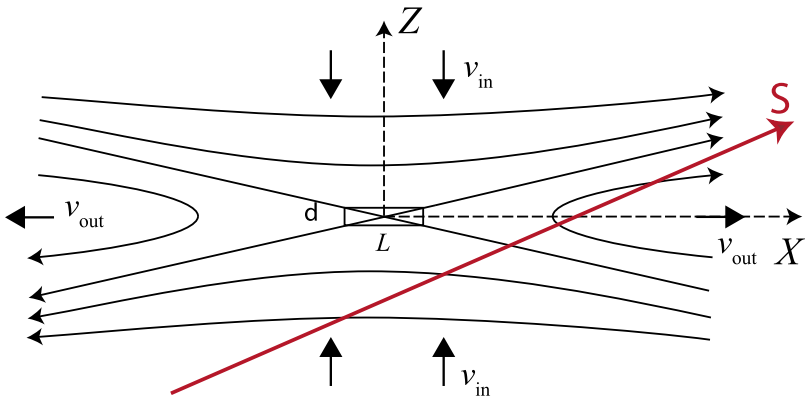

Figure 1. Sketch of reconnection geometry in the magnetotail. The X point is at the origin of the *X*-*Z* (GSM) coordinate system. At large |*Z*|, the reconnecting magnetic field is oriented in the *X* direction. Magnetic flux is transported toward the X point from above and below with speed v_{in}, and away from the X point to the right and left with speed v_{out}. The width δ of the diffusion region (rectangular box), is less than its length *L*, corresponding to greater gradient in the *Z* direction. The path of the centroid of the array of virtual spacecraft is schematically represented by the path S. (The spacecraft separation is small on this scale.)

this paper, we will consider "quasi-two dimensional" reconnection, as illustrated in Figure 1. If a structure is quasi-two dimensional, there will be a direction in which the variation is significantly less than that of the other directions. We call this the "invariant" or "out of plane" direction, recognizing however that in a real three-dimensional system, this invariance is only approximate. In the case of quasi-two dimensional reconnection the equilibrium (large-scale) gradients within the plane shown in the figure will be much larger than the gradients out of the plane. The direction of largest gradient in Figure 1 is across the current sheet, i.e., the *Z* direction ($\boldsymbol{e}_z$) in the figure. The direction of intermediate gradient is along the reconnecting magnetic field, i.e., the *X* direction ($\boldsymbol{e}_x$) in the figure. The direction of minimum gradient is the third (out-of-plane) direction, i.e., the *Y* direction ($\boldsymbol{e}_y$).

[3] *Shi et al.* [2005] developed a method to determine three directions corresponding to maximum, intermediate, and minimum values of the squared magnitude of the vector magnetic field gradient. They called this technique "Minimum Direction Derivative (or Difference)", or MDD, analysis. This method requires field observations from four closely spaced spacecraft in order to determine the gradient. A potential advantage of this method is that it yields the directions at each point in time, thus in principle allowing changes in orientation of a structure to be monitored. According to the method, the gradient of the magnetic field is first calculated, and expressed as the matrix $\mathbf{M}^{\nabla B}$, where $M_{ik}^{\nabla B} = \partial_i B_k$, and ∂_i is the spatial partial derivative in the *i*'th direction. Then the symmetric matrix $\mathbf{M}^{G} \equiv \mathbf{M}^{\nabla B} \cdot (\mathbf{M}^{\nabla B})^{T}$ is formed, where "T" indicates the transpose of the matrix. The three eigenvalues of $\mathbf{M}^{G}$, λ_{G-max}, λ_{G-int}, and λ_{G-min}, represent the maximum, intermediate, and minimum values of the squared directional derivative (gradient), with the eigenvectors $\boldsymbol{e}_{G-max}$, $\boldsymbol{e}_{G-int}$, and $\boldsymbol{e}_{G-min}$ indicating the corresponding directions. As *Shi et al.* [2005] explain, in order for the structure to be roughly two-dimensional, λ_{G-min} should be significantly less than the other two eigenvalues. If $\lambda_{G-max} \gg \lambda_{G-int}, \lambda_{G-min}$, the structure is quasi-one-dimensional. If all the eigenvalues are comparable, the structure is fully three-dimensional, and the eigenvector directions may not be useful for our purposes. *Shen et al.* [2003, 2007a, 2007b] used a similar approach based on the gradient of the magnetic field direction $\boldsymbol{b} \equiv \boldsymbol{B}/B$ (see discussion by *Denton et al.* [2010]). Note that the *Shi et al.* [2005, 2006] method has been used recently to investigate small-scale magnetic structures [*Shi et al.*, 2009a] and the cusp boundary [*Shi et al.*, 2009b].

[4] Assuming time stationarity ($\partial/\partial t = 0$) in the frame of the structure, *Shi et al.* [2006] went on to use $d\boldsymbol{B}/dt$ and $\nabla \boldsymbol{B}$, observed by the four spacecraft to determine the velocity of a structure relative to the spacecraft, $\boldsymbol{V}_{str} = -\boldsymbol{V}_{sc}$, where $\boldsymbol{V}_{sc}$ is the velocity of the spacecraft array relative to the structure,

$$\frac{d\boldsymbol{B}}{dt} = \frac{\partial \boldsymbol{B}}{\partial t} + \mathbf{V}_{sc} \cdot \nabla \boldsymbol{B} = -\mathbf{V}_{str} \cdot \nabla \boldsymbol{B}, \tag{1}$$

They called this technique "Spatio-temporal Difference" analysis, which they abbreviated as STD.

[5] *Denton et al.* [2010] considered the effect of random noise and calibration errors on the *Shi et al.* [2005, 2006] methods. While the effect of noise errors could be eliminated by averaging in time, calibration errors were a more difficult problem to deal with because they systematically contaminate calculation of the gradient $\nabla \boldsymbol{B}$ [*Denton et al.*, 2010]. This is because the magnetic field measured by the spacecraft is the sum of the real magnetic field and the constant (with respect to time) calibration errors, and the gradient of the calibration errors is constant and nonzero, leading to systematic error in the apparent gradient.

[6] In order to eliminate the effect of calibration errors, *Denton et al.* [2010] modified the *Shi et al.* [2005] method by using the perturbed matrix

$$\delta \mathbf{M}^{\nabla B} \equiv \mathbf{M}^{\nabla B} - \langle \mathbf{M}^{\nabla B} \rangle_0, \tag{2}$$

where $\langle \mathbf{M}^{\nabla B} \rangle_0$ is an average value of $\mathbf{M}^{\nabla B}$ ($=\nabla \boldsymbol{B}$) calculated within an interval typically centered on the time at which $\mathbf{M}^{\nabla B}$ has its largest value. This is also the time of largest eigenvalue of $\mathbf{M}^{G}$, since that eigenvalue is the square

of the amplitude of the largest value of $\nabla \boldsymbol{B}$ [*Denton et al.*, 2010]. They then used $\delta \mathbf{M}^{\nabla B}$ for the analysis in the same manner as *Shi et al.* [2005]. Subtracting off the average value of $\mathbf{M}^{\nabla B}$ eliminates the effect of the calibration errors, since these errors lead to a constant gradient. Denton et al. then found the time average $\langle \delta \mathbf{M}^{\mathrm{G}} \rangle$ of the time dependent matrix $\delta \mathbf{M}^{\mathrm{G}} \equiv \delta \mathbf{M}^{\nabla B} \cdot (\delta \mathbf{M}^{\nabla B})^{\mathrm{T}}$, where $\delta \mathbf{M}^{\nabla B} \equiv \mathbf{M}^{\nabla B} - \langle \mathbf{M}^{\nabla B} \rangle_0$. The averaging interval used to calculate $\langle \delta \mathbf{M}^{\mathrm{G}} \rangle$ may be different from that used for $\langle \mathbf{M}^{\nabla B} \rangle_0$. Experience to date indicates that it may be best to average $\langle \mathbf{M}^{\nabla B} \rangle_0$ near the center of the current sheet where the gradient is large, whereas the minimum gradient direction is sometimes best found away from the current sheet [*Denton et al.*, 2010]. Having averaged $\langle \delta \mathbf{M}^{\mathrm{G}} \rangle$, we can then use the eigenvectors of $\langle \delta \mathbf{M}^{\mathrm{G}} \rangle$ to get the gradient directions. By use of shifting averages, slow changes in orientation can in principle still be monitored, although this aspect is not pursued here.

[7] *Denton et al.* [2010] also modified (1) in order to eliminate the effect of calibration errors. Using the average of $\nabla \boldsymbol{B}$ and the average of $d\boldsymbol{B}/dt$ (in the spacecraft frame) over the same time interval, $\boldsymbol{V}_{\mathrm{str}}$ can be found from

$$\delta\left(\frac{d\boldsymbol{B}}{dt}\right) = -\mathbf{V}_{\mathrm{str}} \cdot \delta(\nabla \boldsymbol{B}), \tag{3}$$

where $\delta(d\boldsymbol{B}/dt) \equiv d\boldsymbol{B}/dt - \langle d\boldsymbol{B}/dt \rangle_0$, and $\delta(\nabla \boldsymbol{B}) \equiv \nabla \boldsymbol{B} - \langle \nabla \boldsymbol{B} \rangle_0$.

[8] Using simulated spacecraft observations from four virtual spacecraft flown through an MHD simulation of magnetic reconnection in the geomagnetic tail, *Denton et al.* [2010] tested the direction-finding method [*Shi et al.*, 2005] and the method to determine the structure velocity [*Shi et al.*, 2006]. Employing the gradient calculated from the measured vector magnetic field without calibration errors and noise, they found that these quantities could be well determined. They also showed that these quantities could be well determined even when calibration errors were added, provided that the perturbed quantities were used in the calculations as discussed above. They found that the angles were determined within about 3° and the magnitude of the structure velocity within about 3%.

[9] While the results of *Denton et al.* [2010] are encouraging, there are limitations of the study that we address in this paper. First, the results were derived entirely from a single MHD simulation of reconnection in the magnetotail. We now want to see if the method works for other simulations. The simulation used by Denton et al. was for anti-parallel reconnection (no component of the equilibrium magnetic field in the out of plane $\boldsymbol{e}_Y$ direction). In the present paper, we will test the method for another quasi-two dimensional, anti-parallel MHD reconnection simulation, but we will also test it using an MHD simulation with a guide field and a full dynamics kinetic simulation.

2. Errors

[10] As discussed by *Denton et al.* [2010], in real spacecraft data there are two kinds of errors in magnetic field measurements, digitization (noise) errors that randomly vary with respect to time, and systematic calibration errors that are constant or very slowly evolving with respect to time. For each simulation, following Denton et al., we will add to the virtual spacecraft measurements 0.01 nT time varying noise errors and constant 0.1 nT calibration errors, both randomly chosen for each component of the magnetic field. (For calibration errors of this magnitude, the apparent value of $\nabla \cdot \boldsymbol{B}$ (from the trace of the $\mathrm{M}_{ik}^{\nabla B}$ matrix) is not significantly affected, though it could be for larger calibration errors.) We consider this a worst-case scenario. For Cluster, it is sometimes possible to reduce the calibration errors in the spacecraft spin plane using measurements by the Electron Drift Instrument (EDI) [*Georgescu et al.*, 2006]. For MMS, it should be possible to reduce the relative (between spacecraft) calibration errors (which is crucial for calculating the gradient), taking advantage of time periods for which the magnetic field measured by each spacecraft should be the same because the field is nearly uniform and the spacecraft separation is small (R. Torbert, private communication, 2010). Reduction of the errors will make the calculations more accurate. For the present paper, we will ignore errors associated with calculation of the gradients; basically, the spacecraft configuration needs to be roughly tetrahedral and the scale length for spatial variation needs to be significantly larger than the spacecraft separation in order for the gradients to be calculated accurately.

3. Investigations

[11] *Denton et al.* [2010] considered a snapshot of the MHD fields from a quasi-two-dimensional simulation of reconnection [*Birn and Hesse*, 2009]. On the large scale [*Birn and Hesse*, 2009, Figure 3], the structure was strongly three dimensional, but at the central value of the simulation ($y = 0$ [*Birn and Hesse*, 2009, Figure 3], where y is the cross tail (GSM Y) coordinate), the simulation was approximately two dimensional. That is, their B_y was small compared to the lobe magnetic field and the cross-tail variation was weak compared to the variation in their z (downstream tail coordinate, GSM $-X$). Virtual (simulated) spacecraft were flown across this snapshot (with a path schematically represented by S in Figure 1) so that the only time dependence of the recorded data was due to the motion of the spacecraft. (The spacecraft velocity included components in all three directions including the quasi-two-dimensional "out-of-plane" direction (y direction of Birn and Hesse).) This same method will be used in this paper; that is, real time dependence will not be considered. Therefore, the potential of the Shi et al. method to recover slow time evolution of directions and velocity will not be examined. Anomalous resistivity was used in the region around the X point which was traversed by the spacecraft. The reconnecting magnetic field (the X component) was 20 nT and the proton density was of order 0.08 cm^{-3} in the current sheet, and 0.05 cm^{-3} in the upstream (inflow) region. The plasma beta was small $\sim 10^{-3}$ to 10^{-2} in the inflow region, but large $\gg 1$ at the current sheet. This simulation had approximately zero guide field (zero Y component of $\boldsymbol{B}$ in the midnight meridian plane). Here we will first consider data from two other MHD simulations with similar parameters.

3.1. MHD Simulation With Zero Guide Field

[12] Run 1 is very much like the simulation considered by *Denton et al.* [2010]; it also does not have a guide field. The main difference between the two simulations is that the length scale in the new simulation is smaller (200 km versus

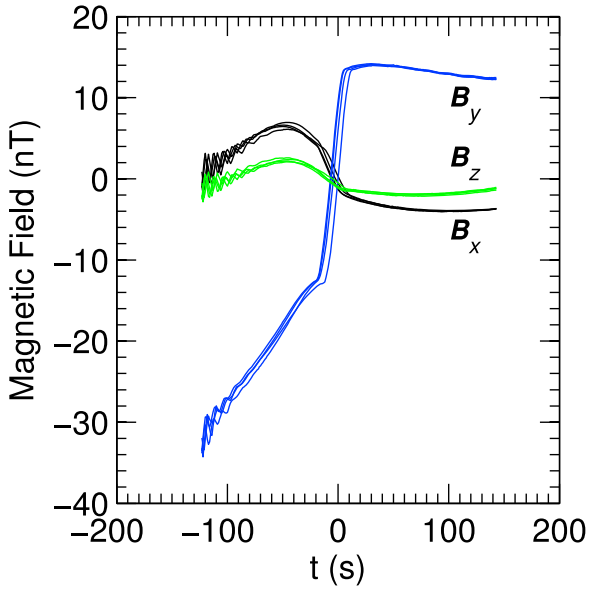

Figure 2. The x (black), y (blue), and z (green) components (rotated in an arbitrary way relative to the natural simulation coordinates) of the magnetic field for all four virtual spacecraft flown through the snapshot of the magnetic field from Run 1.

1000 km), so that the crossing of the current sheet is faster and there are consequently fewer data points during the crossing. Before analyzing the data, we add 0.01 nT random noise error (varying with time) and 0.1 nT systematic calibration errors (constant with respect to time) to each component of the magnetic field. The data were sampled at a time resolution of 1.0 s. Figure 2 shows the magnetic field measurements in (arbitrary) simulation coordinates for all four virtual spacecraft. The fact that the four curves for each component do not vary greatly (the blue curves, for instance, are almost exactly superposed) indicates that the separation of the spacecraft (100 km here) is small relative to the global spatial scales. To implement the *Shi et al.* [2005] method using the perturbed magnetic field developed by *Denton et al.* [2010], we first need to identify the region of the largest gradient, which occurs when the central current sheet is crossed at approximately $t = 0$. Figure 3 shows the three eigenvalues, λ_{G-max} (black), λ_{G-int} (blue), and λ_{G-min} (green) using the matrix $\mathbf{M}^{\nabla B}$ based on the gradient of the unperturbed magnetic field after doing a running average of the magnetic field values at each time using the values within ±5 s (11 measurements) in order to reduce the effects of noise. The peak in λ_{G-max} occurs at about $t = -3$ s. Using a procedure to be discussed shortly, we chose a time segment between −41.5 s and 34.5 s for the purpose of calculating $\langle \mathbf{M}^{\nabla B} \rangle_0$ in order to get $\delta\mathbf{M}^{\nabla B}$ using (2).

[13] Figure 4a shows the eigenvalues using the perturbed gradient matrix $\delta\mathbf{M}^{\nabla B}$, again after doing a running average of the magnetic field values at each time using the values within ±5 s. As mentioned in the Introduction, averaging the data helps to eliminate problems related to random noise, whereas using the perturbed gradient $\delta\mathbf{M}^{\nabla B}$ eliminates the problem of calibration errors. Note that the maximum gradient eigenvalue λ_{G-max} (black) in Figure 4a is now much lower in the central region, because we have subtracted off the average gradient within this region. Nevertheless, this eigenvalue is still significantly higher than the other eigenvalues except at two times where λ_{G-max} plummets to small values; this is where the value of λ_{G-max} based on the unperturbed gradient approaches the average value of the gradient within the central region. Figures 4b–4d show the direction cosines for the maximum gradient direction $\boldsymbol{e}_{G-max}$, the intermediate gradient direction $\boldsymbol{e}_{G-int}$, and the minimum gradient direction $\boldsymbol{e}_{G-min}$. The gradient directions are specified by the direction cosines with respect to the x (black), y (blue), and z (green) directions. For the MHD simulations, this (x, y, z) coordinate system was rotated in an arbitrary way relative to the original simulation coordinates to see if the latter could be recovered in blind tests.

[14] As suggested by *Denton et al.* [2010], there are two guidelines for picking a section of time within which to calculate the gradient directions. We look for a period of time during which there is a large separation in the gradient eigenvalues (Figure 4a) and during which there is also stability to the gradient directions (Figures 4b–4d). These criteria are fairly well satisfied in the right half of the plot from t = 40 to 140 s. Using this time interval, we calculate the average perturbed gradient matrix $\langle \delta\mathbf{M}^{\nabla B} \rangle$ and then get the eigenvalue directions using this matrix. The direction cosines relative to the simulation (x, y, z) coordinate system calculated using this average matrix are the filled circles (dots) plotted in Figures 4b–4d, where the colors have the same meaning as for plotting the instantaneous direction cosines. Clearly the direction cosines based on the average matrix are consistent with the values calculated using the instantaneous gradient $\delta\mathbf{M}^{\nabla B}$ during this time interval (t = 40 to 140 s). These directions are 2.7, 4.4, and 3.5° off from the presumed exact directions. (Since the actual simulation

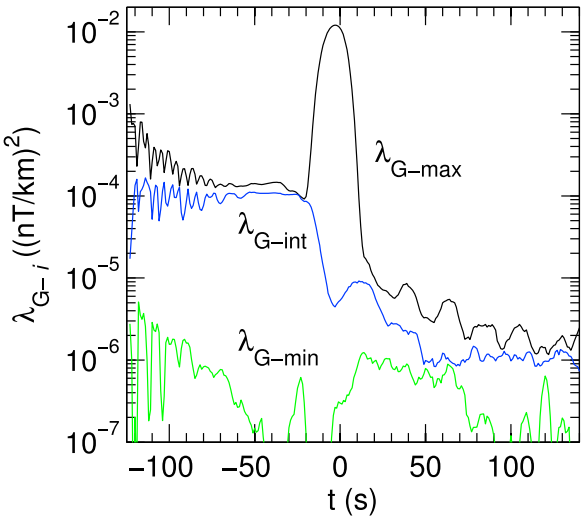

Figure 3. Maximum gradient (black), intermediate gradient (blue), and minimum gradient (green) eigenvalues, λ_{G-i}, versus time in seconds for Run 1 using the matrix $\mathbf{M}^{\nabla B}$ based on the gradient of the unperturbed magnetic field.

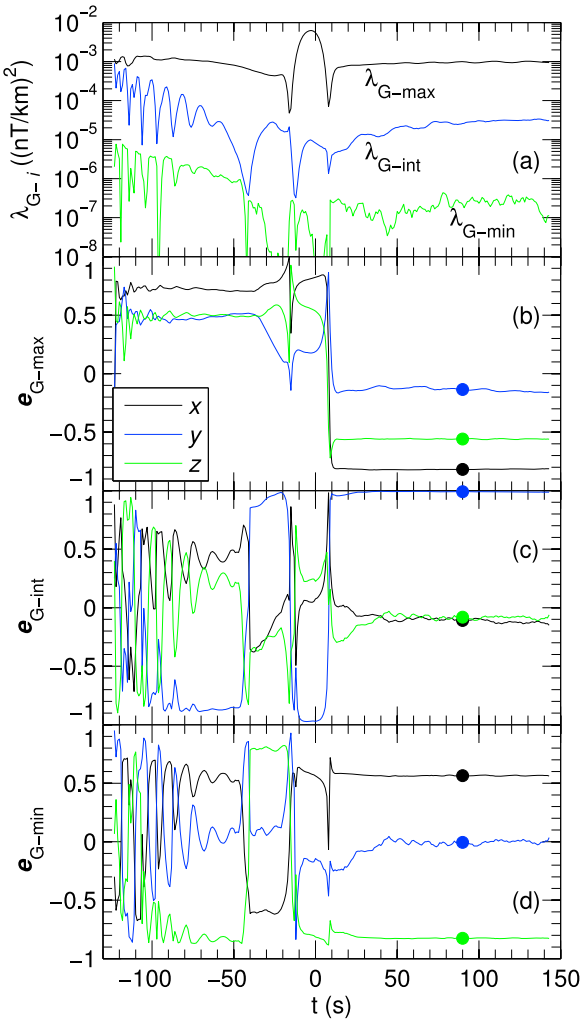

Figure 4. (a) Eigenvalues λ_{G-i} as in Figure 3, except using the perturbed matrix $\delta M^{\nabla B}$, (b) maximum gradient direction $\boldsymbol{e}_{G-max}$, (c) intermediate gradient direction $\boldsymbol{e}_{G-int}$, and (d) minimum gradient direction $\boldsymbol{e}_{G-min}$, all versus time for Run 1. The gradient directions are specified by the direction cosines with respect to the x (black), y (blue), and z (green) directions. The filled circles (dots) indicate the directions cosines found using the perturbed gradient matrix $\langle \delta M^{\nabla B} \rangle$ averaged from $t = 40$ to 140 s.

was only quasi-two-dimensional, the exact simulation maximum gradient, intermediate gradient, and minimum gradient directions are not known with precision.) These errors are listed in Table 1.

[15] Now we return to the question of how to determine the time interval for averaging $\langle \mathbf{M}^{\nabla B} \rangle_0$. *Denton et al.* [2010] suggested that the time interval should encompass the region of maximum gradient. This is the region where the reconnection magnetic field changes rapidly within the "magnetic island", the region of reconnected magnetic flux shown, for instance, in Figure 1. They showed [*Denton et al.*, 2010, Table 1] that the results for the directions were relatively insensitive to the averaging interval. The results became somewhat worse if a very large averaging interval was used; the accuracy for small averaging intervals wasn't explored. Now we attempt to find a systematic method to determine a good averaging interval.

[16] We first identify the largest range of time for which the time-dependent maximum gradient is within half of its maximum value maximized with respect to time, i.e., the time range for which the black curve in Figure 3 is within a factor of 4 of its largest value (note that the eigenvalue is the square of the gradient). Then we examine the error in the minimum gradient direction (which direction is often difficult to find; the maximum gradient direction can usually be found from the unmodified *Shi et al.* [2005] method) for different time intervals centered on the midpoint of this time interval. The range of time used, Δt_{range}, can be specified by the ratio $\Delta t_{range}/\Delta t_{half}$, where Δt_{half} is the previously defined time range encompassing the region for which the maximum gradient is half of its maximum value. We use the same time range $t = 40$ to 140 s for evaluating the average perturbed gradient matrix $\langle \delta \mathbf{M}^{\nabla B} \rangle$, from which we evaluate the gradient directions, in each case. Figure 5a shows the angle $\angle(\boldsymbol{e}_{G-min}, \boldsymbol{e}_Y)$ between the minimum gradient direction $\boldsymbol{e}_{G-min}$ and the presumed exact direction $\boldsymbol{e}_Y$. While there are possibly fortuitous choices of small averaging intervals, the presumed error $\angle(\boldsymbol{e}_{G-min}, \boldsymbol{e}_Y)$ becomes consistently small only for $\Delta t_{range}/\Delta t_{half} \geq 2$. The choice of −41.5 s and 34.5 s for the averaging interval mentioned earlier represented $\Delta t_{range}/\Delta t_{half} = 4$. (Figure 5b is discussed in Section 3.2, the bold curve of Figure 5c is discussed in Section 3.3, and the thin curves of Figure 5c are discussed in Section 4.)

[17] While in our experiments we know the desired answer, i.e., the $\boldsymbol{e}_Y$ direction, this will not be known when we are dealing with real spacecraft data. But Figure 5a suggests that we can use a time interval for the average gradient that is large enough such that the minimum gradient direction converges to some stable answer.

[18] For comparison, if we instead use the unperturbed matrix $\mathbf{M}^{\nabla B}$ based on $\boldsymbol{B}$ with errors within the time interval $t = -10$ to 10 s in Figure 3, during which time the separation in the three eigenvalues is largest, the eigenvector directions from the average matrix are 1.0, 35.6, and 35.6° off from the exact directions. This shows that the maximum gradient

Table 1. Angular Difference Between Directions $\boldsymbol{e}_{G-max}$, $\boldsymbol{e}_{G-int}$, and $\boldsymbol{e}_{G-min}$ Inferred by the Modified *Shi et al.* [2005] Method Using the Perturbed Gradient, and the Corresponding Approximate (for Quasi-Two-Dimensional MHD Simulations) or Exact (for Exactly Two-Dimensional Kinetic Simulation) Directions, $\boldsymbol{e}_Z$, $\boldsymbol{e}_X$, and $\boldsymbol{e}_Y$

Run	Equations	Guide Field	Time Range (s)	$\angle(\boldsymbol{e}_{G-max}, \boldsymbol{e}_Z)$[a]	$\angle(\boldsymbol{e}_{G-int}, \boldsymbol{e}_X)$[a]	$\angle(\boldsymbol{e}_{G-min}, \boldsymbol{e}_Y)$[a]
1	MHD	no	40 to 140	2.7°	4.4°	3.5°
2	MHD	yes	−700 to −500	3.9°	3.7°	3.1°
3	Kinetic	no	150 to 190	2.6°	2.7°	1.9°

[a]Angle between the argument vectors.

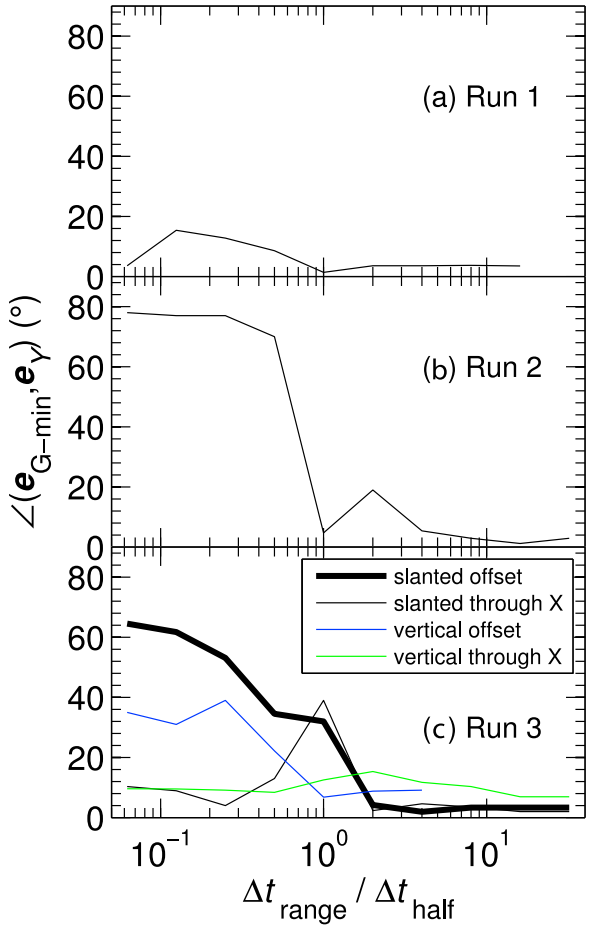

Figure 5. Angle $\angle(\boldsymbol{e}_{G-min}, \boldsymbol{e}_Y)$ between the minimum gradient direction $\boldsymbol{e}_{G-min}$ and $\boldsymbol{e}_Y$ versus the normalized time range $\Delta t_{range}/\Delta t_{half}$ used for averaging $\langle M^{\nabla B}\rangle_0$ as described in the text for (a) Run 1, (b) Run 2, and (c) Run 3 (thick black curve). In Figure 5c, the thin curves show variations of Run 3; the thin black curve is for the spacecraft passing through the X point with same velocity as was used for Run 3, the blue curve is for spacecraft velocity in the Z direction crossing the current sheet about 20 c/ω_{pi} downstream of the X point, and the green curve is for the spacecraft relative velocity in the Z direction passing through the X point.

direction can be accurately determined using the unperturbed matrix, but the minimum gradient direction can only be well determined (at least with the *Shi et al.* [2005] method) using the perturbed matrix if the calibration errors are large. The effect of calibration errors on the unmodified method will be examined more thoroughly in the Discussion section. As mentioned by *Denton et al.* [2010], comparison of the directions using the unperturbed and perturbed matrix can help to establish whether or not the calibration errors are significant.

[19] Now we calculate the structure velocity $\boldsymbol{V}_{str}$ using the data from Run 1, again with 0.01 nT random noise errors and 0.1 nT systematic calibration errors added to each component of the magnetic field. In order to calculate $\boldsymbol{V}_{str}$, we use the perturbed gradient and perturbed time derivative as described by (3) with the same time interval for averaging as was used for determining the directions. Before calculating the gradients and time derivative of the magnetic field, the magnetic field values were averaged at each point in time over a time interval of ±5 s (11 data points) as before.

[20] Figure 6 shows the results for the inferred velocity components versus time (curves) and the exact values of the components from the simulation (dotted horizontal lines). The components of the spacecraft measurements in the x, y, and z coordinate directions are indicated by black, blue, and green color, respectively. As was done by *Denton et al.* [2010], we determine the total structure velocity $\boldsymbol{V}_{str}$, not just the "in-plane" components. This is possible because the simulation was weakly three-dimensional and the gradient in the minimum gradient direction was large enough so that the component of the velocity in that direction could be well determined. Evidence that the total velocity is reliable is that the components of $\boldsymbol{V}_{str}$ in Figure 6 are relatively stable (except in the vicinity of the spike in $\boldsymbol{V}_{str}$ components at $t \sim 0$ where the minimum gradient is particularly small; see Figure 3a). While we were able to determine all three components of the structure velocity in this case, it should be kept in mind that the component of the velocity in the minimum gradient direction could be inaccurate [*Shi et al.*, 2006].

[21] Median values of the velocity components were determined between $t = 35$ s and $t = 125$ s, during which time the velocity components were particularly stable. The median values are plotted in Figure 6 as the filled circles. The magnitude of the inferred velocity is accurate to 1.6%, and the direction is accurate to within 5.2°. These values are listed in Table 2. (Comparable values could be found by using a time range which included the sharp peaks in Figure 6 as was done by *Denton et al.* [2010]; using the median values excludes the extreme values within the peaks.)

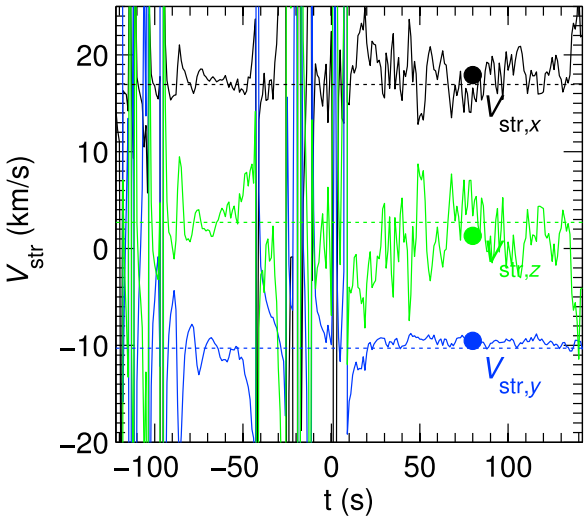

Figure 6. Run 1 spacecraft measurements x (black curve), y (blue curve), and z (green curve) components (arbitrary coordinate system) of the structure velocity $\boldsymbol{V}_{str}$ versus time, found from the *Shi et al.* [2006] method modified by using the perturbed gradient and time derivative of $\boldsymbol{B}$. The filled circles show the median values of the curves using the data between $t = 35$ s and 125 s, while the dotted horizontal lines show the exact values from the simulation.

Table 2. Difference $\Delta(V_{str}, V_{str}^{\nabla B})$ Between the Magnitude of the Actual Structure Velocity V_{str} and That Inferred Using ∇B, $V_{str}^{\nabla B}$, and the Angular Difference $\angle(\boldsymbol{e}_{Vstr}, \boldsymbol{e}_{Vstr}^{\nabla B})$ Between $\boldsymbol{e}_{Vstr}$ and $\boldsymbol{e}_{Vstr}^{\nabla B}$ for the Cases Indicated

Run	Equations	Guide Field	Time Range (s)	$\Delta(V_{str}, V_{str}^{\nabla B})$	$\angle(\boldsymbol{e}_{Vstr}, \boldsymbol{e}_{Vstr}^{\nabla B})$
1	MHD	no	35 to 125	1.6%	5.2°
2	MHD	yes	−700 to −200	1.5%	0.9°
2	Kinetic	no	150 to 180	0.08%	1.8°

3.2. MHD Simulation With a Guide Field

[22] Run 2 is also quasi-two-dimensional. It differs from Run 1 in that it has a guide field (a component of B in the "out of plane" direction) of about half the magnitude of the reconnecting field. Again we add 0.01 nT random noise error and 0.1 nT systematic calibration errors to each component of the magnetic field. Next we subtract the average gradient within $t = -68$ and $t = 60$ s to determine the perturbed gradient. In order to make this choice, we examined the presumed error in the minimum gradient direction in a similar manner as was done for Run 1. The results corresponding to $\Delta t_{range}/\Delta t_{half} = 8$ are shown in Figure 5b. (As was mentioned in reference to Run 1, when we are analyzing spacecraft data we will not know the Y direction, so in practice, we will need to look for convergence of the minimum gradient direction.) Figure 7a shows the eigenvalues of the maximum, intermediate, and minimum gradient directions for Run 2, while Figures 7b–7d show the corresponding direction cosines (as for Run 1). Again, we look for a time interval during which the eigenvalues for the gradient directions (Figure 7a) are well separated and the eigenmode directions are relatively steady. Picking the time period between $t = -700$ and -500 s, we find the components (black, blue, and green for x, y, and z, respectively) of each eigenmode direction; these are plotted as the filled circles in Figures 7b–7d. These directions are 3.9° 3.7° and 3.1° off from the presumed extremal gradient directions in the simulation; these values are listed in Table 1. As mentioned in reference to Run 1, the true directions are not exactly known because the simulation is only approximately two-dimensional. If we instead choose the time period $t = 40$ to 90 s, for which the eigenvalues are better separated (Figure 4a), but the directions are less steady (Figures 7b–7d), we find that the directions are 5.8°, 7.0°, and 5.4° off from the presumed true directions.

[23] If we do not add any random or calibration errors to the simulation data, and use the unmodified *Shi et al.* [2005] method, we get the results shown in Figure 8. In this case, it is not possible to use the same time interval to find the maximum and minimum gradient directions. Using the central time interval, $t = -15$ to 5 s, where the maximum gradient eigenvalue (black curve in Figure 8a) is extremely large, we can find the maximum gradient direction $\boldsymbol{e}_{G-max}$ with an error of 3.4° from the presumed direction. Then using the interval $t = 120$ to 260 s, during which the minimum gradient eigenvalue λ_{G-min} (green curve in Figure 8a) is much lower than the other eigenvalues, and during which the minimum gradient eigenmode direction $\boldsymbol{e}_{G-min}$ is relatively steady (Figure 8d), we can find the minimum gradient direction with an approximate error of 5.7° from the presumed direction. If we then get the intermediate gradient direction as the renormalized cross product $\boldsymbol{e}_{G-min} \times \boldsymbol{e}_{G-max}$, we find the presumed errors in the three directions to be 3.4°, 1.0°, and 4.1°, respectively, for the maximum, intermediate, and minimum gradient directions.

[24] Comparison of Figures 7 and 8 shows an interesting fact. Subtracting off the maximum gradient near the peak of the maximum gradient ($t \sim 0$ in Figure 8a) has the effect of introducing a larger maximum gradient (in that direction) at times away from the peak (times different than $t \sim 0$ in Figure 4a; note that the black curve is almost uniformly at a large value). So, in addition to subtracting off constant gradients that would result from calibration errors, the modified *Shi et al.* [2005] method using the perturbed gradient transfers information about the maximum gradient to times away from its peak value.

[25] Now we calculate the structure velocity $\boldsymbol{V}_{str}$ using the data from Run 2 with 0.01 nT random noise error and 0.1 nT systematic calibration error added to each component of the magnetic field. We then smooth the data at each time using a time interval ±50 s (101 data points) and use the perturbed

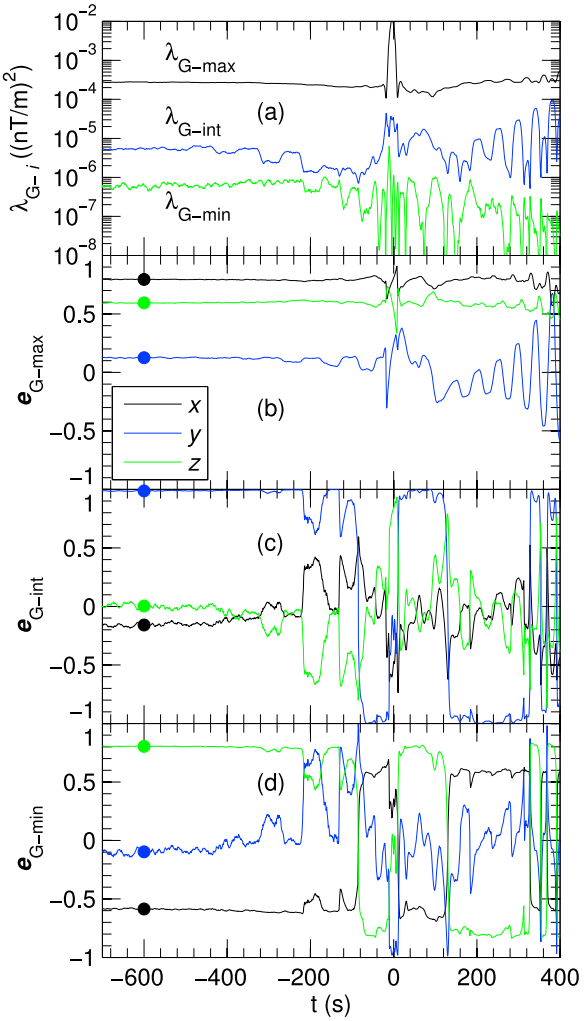

Figure 7. Same as Figure 4, except Run 2 (MHD with a guide field). The filled circles indicate the directions cosines found using the perturbed gradient matrix $\langle \delta \mathbf{M}^{\nabla B} \rangle$ averaged from $t = -700$ s to -500 s.

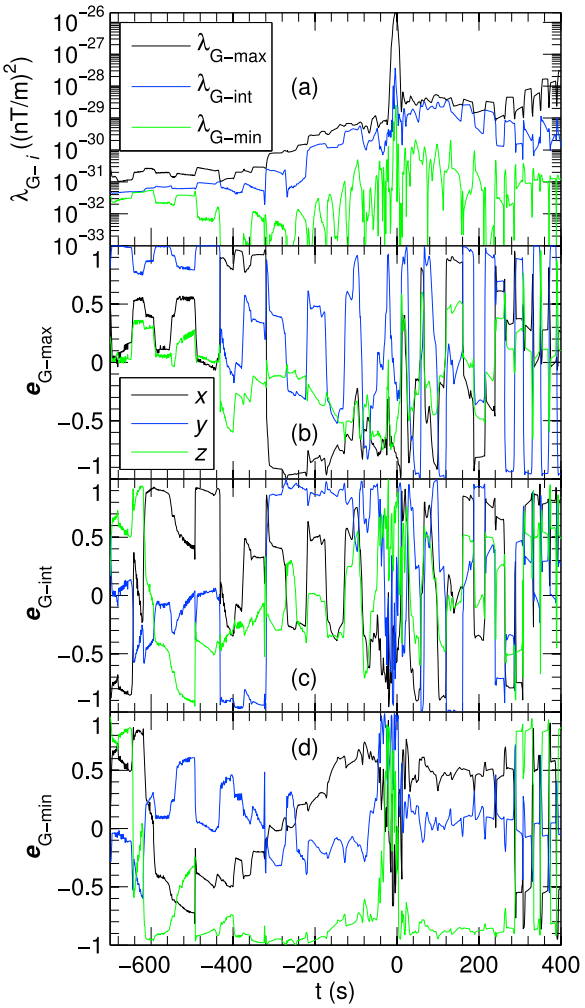

Figure 8. Same as Figure 7, except for Run 2 with no magnetic field errors added, and analyzed using the unmodified *Shi et al.* [2005] method.

gradient and perturbed time derivative as described by (3) to calculate $\boldsymbol{V}_{str}$. The results are shown in Figure 9 for the entire velocity $\boldsymbol{V}_{str}$, again not subtracting off the component of $\boldsymbol{V}_{str}$ in the minimum gradient direction. The clue that we are able to obtain a reliable result is again that all 3 velocity components in the plots are steady (Figure 9). Figure 9 shows the results for the inferred velocity components versus time (curves) and the exact values of the components from the simulation (dotted horizontal lines). The median values of the velocity components were determined between $t = -700$ and -200 s, and are plotted in Figure 9 as the filled circles. The magnitude of the inferred velocity is accurate to 1.5%, and the direction is accurate to within 0.9°. These values are listed in Table 2.

[26] Figure 10 shows the inferred structure velocity $\boldsymbol{V}_{str}$ using the same method, but with a smoothing interval of ±5 s instead. The results are similar, but more noisy.

3.3. Full Dynamics Kinetic Simulation

[27] Now we consider results from an array of virtual spacecraft flying through a two-dimensional full dynamics kinetic simulation of the magnetotail. This simulation was described by *Shay et al.* [2007] and *Drake et al.* [2009]. In this case, referred to as Run 3, the simulation is truly two-dimensional. While there is no constant guide field, there is a significant spatially varying Hall magnetic field in the out of plane direction, with magnitude about half that of the reconnection magnetic field immediately upstream of the current sheet. The kinetic simulation used normalized units; for the purposes of comparison and more easily relating to the real situation in the magnetotail, we convert the normalized units to real units by multiplying values of B by 15 nT, values of time by (1/1.5) s, values of velocity by 1500 km/s, and values of distance by 1000 km. If the fields were exactly known, it would be possible to find the direction along which there was exactly zero gradient. The simulation, however, has numerical noise due to the particle distribution. We estimate the amplitude of this numerical noise level to be at least 0.005 nT. In order to bring the noise level up to 0.01 nT, we add additional time-dependent random noise (time-dependent) of 0.009 nT (from $\sqrt{(0.01)^2 - (0.005)^2}$) to each component of the magnetic field. In addition, we also add random time independent calibration errors to the components of the magnetic field at the level of 0.1 nT. The data were sampled at a time resolution of 0.1 s, and the effect of noise errors could be eliminated with a smaller averaging interval; we used ±3 s.

[28] The interval used to determine the average gradient, t = 70 to 120 s, was chosen in the same way as for Runs 1 and 2. The error in the minimum gradient direction is shown versus the averaging interval as the thick black curve in Figure 5c. We chose $\Delta t_{range}/\Delta t_{half} = 4$.

[29] Figure 11a shows the eigenvalues of the maximum, intermediate, and minimum gradient directions for Run 3, while Figures 11a–11d show the corresponding direction cosines using the modified *Shi et al.* [2005] method.

[30] The eigenvalues are well separated and the directions are stable in the early and late stages of the simulation. Using the time period between 150 and 190 s, we find directions that are 2.6°, 2.7°, and 1.9° off from the exact directions

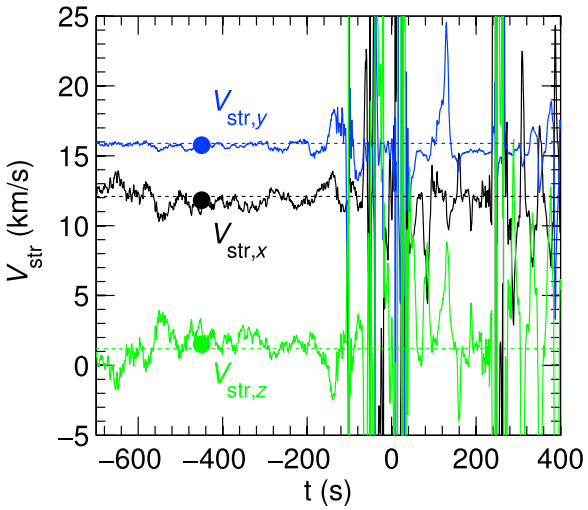

Figure 9. Like Figure 6, except for Run 2. The filled circles show the median values of the curves using the data from $t = -700$ s to -200 s.

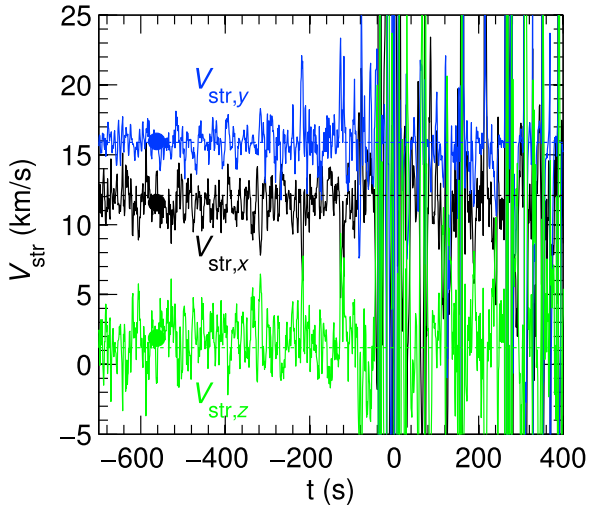

Figure 10. Same as Figure 9, but with the smoothing interval for the magnetic field reduced to ±5 s.

(because this simulation is precisely two-dimensional); these values are listed in Table 1. In this case, the $\boldsymbol{e}_x$, $\boldsymbol{e}_y$, and $\boldsymbol{e}_z$ spacecraft measurements directions are the same as the simulation directions $\boldsymbol{e}_X$, $\boldsymbol{e}_Y$, and $\boldsymbol{e}_Z$, respectively (the coordinate axes have not been rotated). Clearly, these directions are very well determined by the modified *Shi et al.* [2005] method.

[31] If we calculate the eigenvalues and directions using the unmodified *Shi et al.* [2005] method instead, but still including random and calibration errors, the directions (not shown) are not very steady for any time period. The most stable directions occur near the peak in the gradient, but the intermediate and minimum gradient directions found using that time interval are off from the actual directions by about 88°. The maximum gradient direction is accurate to within 1.5°. This again shows that calibration errors at a level of 0.1 nT severely corrupt information about the intermediate and minimum gradient directions (which have relatively small contributions to the total gradient, compared to the maximum gradient direction), but do not significantly contaminate information about the maximum gradient direction.

[32] Figure 12 shows the same data as in Figure 11, except that here the unmodified *Shi et al.* [2005] method is used for the Run 3 data without errors. The filled circles in Figures 12b–12d show the directions plotted in Figure 11 using the modified method; these directions are within about 3° of the exact directions (Table 1), as was discussed previously. This figure also shows some of the features we have discussed previously. The maximum eigenvalue direction is steady and pointing in the $\boldsymbol{e}_z$ (=$\boldsymbol{e}_Z$) direction (the green curve in Figure 12b is close to unity) within the central time region from about t = 70 to 125 s, where the maximum gradient is large (the black curve in Figure 12a is well above the blue and green curves). The correct direction of the minimum gradient is the $\boldsymbol{e}_y$ (=$\boldsymbol{e}_Y$) direction, as indicated by the blue curve in Figure 12d being near plus or minus 1 (there is an arbitrary 180° ambiguity in the direction). The minimum gradient direction in Figure 12d is seen to be accurate in the early (before 50 s) and late (after 125 s) times. These intervals correspond to the times during which the minimum gradient eigenvalue (green curve in Figure 12a) is significantly lower than the other eigenvalues (blue and black curves in Figure 12a). During the period of large maximum gradient, the minimum gradient direction from the unmodified *Shi et al.* [2005] method is not steady, indicating that the best time periods for determining the minimum gradient direction are at early or late times.

[33] Now we calculate the structure velocity for Run 3 using the modified *Shi et al.* [2006] method, again including calibration and noise errors. Since Run 3 is truly two-dimensional, the gradient in the out of plane direction is exactly zero. Therefore the out of plane component of $\boldsymbol{V}_{str}$ is arbitrary, and cannot be found from (3), except as determined by the noise. Figure 13 shows the results for $\boldsymbol{V}_{str}$ using (3) to determine only the components in the maximum and intermediate gradient directions. As described earlier, we average the gradients and $d\boldsymbol{B}/dt$ in the interval t = 70 to 120 s and also smooth the fields over an interval of approximately ±30 s (increasing this averaging interval does not significantly improve the results). Figure 13 shows that

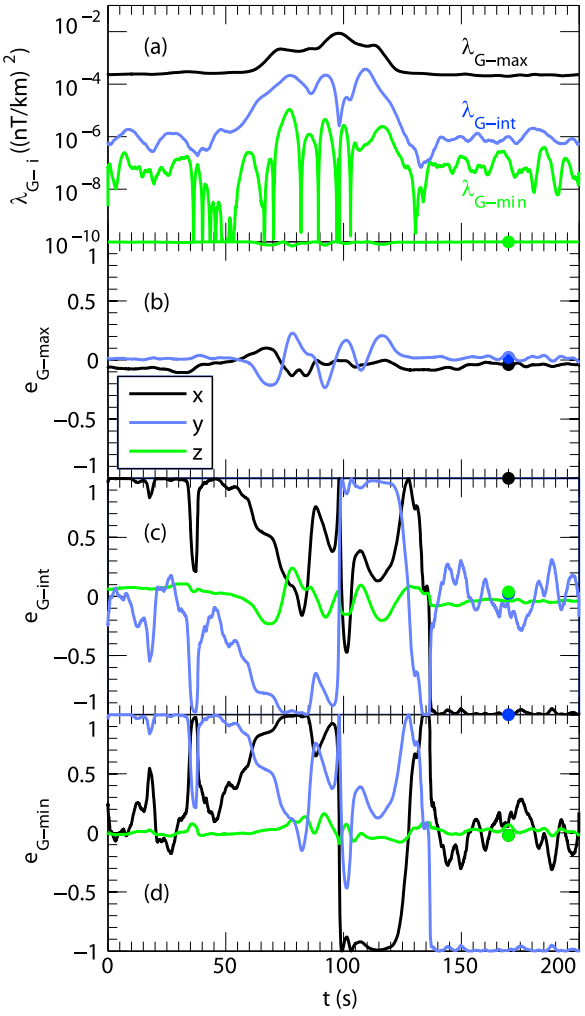

Figure 11. Same as Figure 4, except for Run 3 (the full dynamics kinetic simulation). The filled circles indicate the directions cosines found using the perturbed gradient matrix $\langle \delta \mathbf{M}^{\nabla B} \rangle$ averaged from t = 150 s to 190 s.

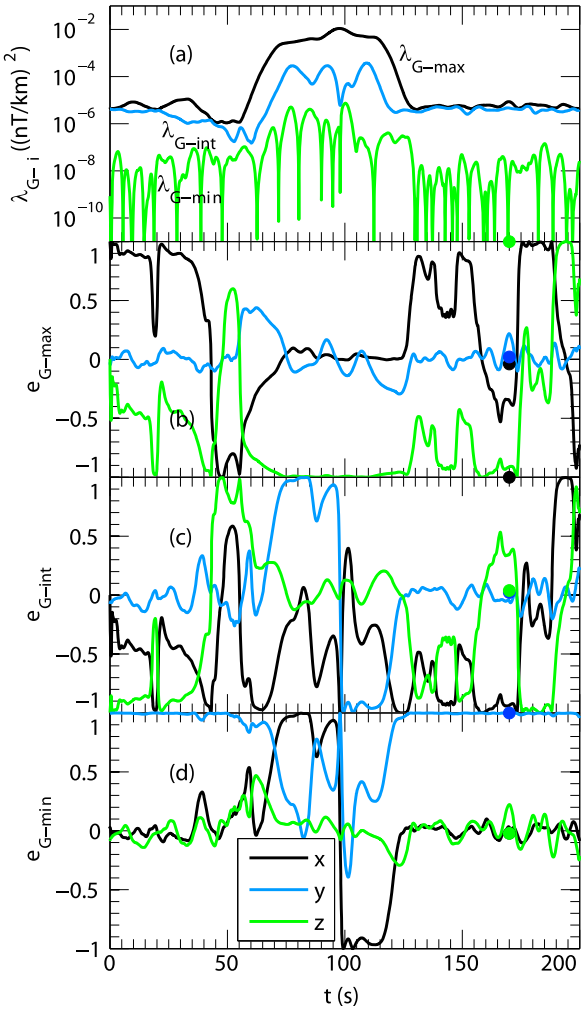

Figure 12. Same as Figure 11, except that the unmodified *Shi et al.* [2005] method (using the total gradient of $\boldsymbol{B}$) is used for the Run 3 data with no magnetic field errors added. The filled circles in Figures 12b–12d show the directions from Figure 11, i.e., from the modified method, again for t = 150 s to 190 s.

the in plane components of $\boldsymbol{V}_{str}$ (black and green curves) are well determined. The median values in the interval 150 to 180 s are plotted as filled circles, and agree well with the exact values (horizontal lines), with an error of 0.08% in magnitude and 1.8° in direction. These values are listed in Table 2. Note that $\boldsymbol{V}_{str,y}$ in Figure 13 (blue curve) is not exactly zero because the minimum gradient direction used to subtract off the minimum variance component of $\boldsymbol{V}_{str}$ is the one that we calculated and not the exact Y direction (here the y direction).

[34] Figure 14 shows the results if we try to determine all three components of $\boldsymbol{V}_{str}$. The x and z (in plane) components of $\boldsymbol{V}_{str}$ determined from (3) (black and green curves, with median values shown for the time interval t = 150 to 180 s as filled circles) again agree well with the exact values (dotted horizontal lines) but the out of plane component $\boldsymbol{V}_{str,y}$ (blue curve in Figure 14) is not accurate, despite the fact that it appears to be steady from t = 150 s to 180 s (though not at earlier times). It should have the same value as the z component (green curve). This indicates that caution should be used when interpreting the minimum gradient component of the structure velocity, at least using the modified *Shi et al.* [2006] method. (For the unmodified method, the y component of $\boldsymbol{V}_{str}$ varies wildly at all times (not shown), clearly indicating that it is not meaningful.)

4. Discussion and Summary

[35] We have shown that the *Shi et al.* [2005, 2006] methods can be successfully used to determine the reconnection geometry and structure velocity $\boldsymbol{V}_{str}$ relative to the spacecraft, even when calibration and noise errors are present, provided that the perturbed gradient is used as described in Section 1. This was shown in Section 3.1 for an MHD simulation without a guide field similar to that examined by *Denton et al.* [2010], in Section 3.2 for an MHD simulation with a guide field, and in Section 3.3 for a full dynamics kinetic simulation that did not have a constant guide field, but did have a Hall magnetic field in the out of plane direction. The agreement between the inferred directions and the approximate true directions (for quasi-two-dimensional simulations) or the exact directions (for the two-dimensional simulation) was good (all within 5°, as shown in Table 1). The structure velocity could also be well determined (magnitude within 2% and direction within 5°, as shown in Table 2).

[36] The maximum gradient and the associated large eigenvalue of the gradient matrix occurs generally at the center of the current sheet crossing, whereas the minimum eigenvalue is most distinct from the intermediate eigenvalue away from the central current sheet crossing (Figures 3 and 12). Thus if the unmodified *Shi et al.* [2005] method is used to determine the reconnection geometry, our results suggest that the maximum gradient direction may be best determined near the central current sheet, while the minimum

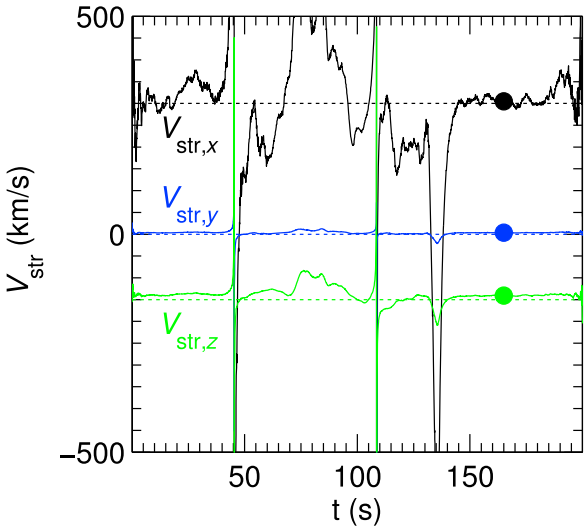

Figure 13. Like Figure 6, except for Runs 3. The components of the velocity are determined only in the maximum-intermediate gradient plane. The filled circles show the median values between t = 150 s and 180 s.

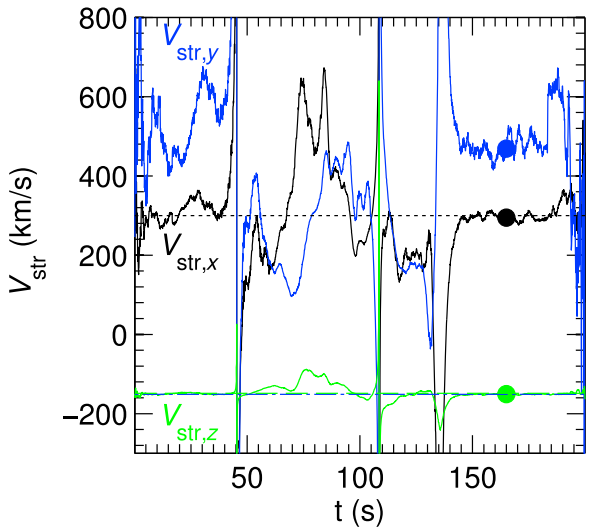

Figure 14. Like Figure 13 for Run 3, except that now all the components of the velocity are determined. The filled circles show the median values between t = 150 s and 180 s.

gradient direction may be best determined away from the central current sheet.

[37] To use the modified *Shi et al.* [2005, 2006] methods, we need to subtract the average gradient from a particular time interval. In agreement with results of *Denton et al.* [2010], we find that a good choice for the subtracted term $\langle \mathbf{M}^{\nabla B} \rangle_0$ in (2) is the average gradient near the central current sheet crossing. Examination of Figures 3 and 12 shows that the maximum eigenvalue tends to be best separated in magnitude from the other eigenvalues (intermediate and minimum) in this region, and that the minimum and intermediate eigenvalues are often least well separated. This means that, at the central current sheet crossing, the reconnection structure tends to be more one dimensional than at other locations. After subtracting the gradient in the central current sheet, information about that gradient direction is transferred to regions far from the central current sheet (Figures 4a, 7a, and 11a), so that an interval away from the central current sheet can then be used to determine all three directions (Section 3.1).

[38] The structure velocity $\boldsymbol{V}_{str}$ can also be determined using the modified *Shi et al.* [2006] method. If the structure is three-dimensional, we are able to determine all three components of the velocity (Figures 6 and 9), but if the minimum gradient is very small (such as occurs exactly for a true two-dimensional system), the minimum gradient component of the structure velocity will not be well determined. In that case we can only get the "in-plane" components of $\boldsymbol{V}_{str}$ (Figures 13 and 14). Noise errors lead to noise in the inferred values of $\boldsymbol{V}_{str}$ (Figure 10 versus Figure 9). The time resolution of the magnetic field instrument is greater for CLUSTER (1/67 s^{-1} time resolution [*Balogh et al.*, 1997]) and even greater for MMS (0.01 s resolution for the fluxgate instrument), than what we have assumed here (between 0.1 and 1 s). We therefore conclude that digital noise errors are unlikely to be a problem.

[39] In all the cases we have studied up to this point, the virtual spacecraft passed to the side of the X point as schematically illustrated in Figure 1. For the full dynamics kinetic simulation, we tried some variations of the spacecraft trajectory. For Run 3, the spacecraft trajectory was at an angle of about 27° to the current sheet and passed about 20 c/ω_{pi} (assumed to be ~20,000 km) in the outflow downstream of the X point. The thin black curve in Figure 5c shows the error as a function of the averaging interval if the spacecraft trajectory is at the same angle to the current sheet but now shifted in the X direction so as to pass through the X point. The blue curve in Figure 5c shows the error as a function of the averaging interval if the spacecraft trajectory is normal to the current sheet (in the Z direction) and crosses the current sheet about 20 c/ω_{pi} downstream of the X point. The green curve in Figure 5c shows the error as a function of the averaging interval if the spacecraft trajectory is normal to the current sheet (in the Z direction) and crosses the current sheet through the X point. Though some of the errors in Figure 5c (~10°) are somewhat larger than those in Table 2 (<5°), it appears that the modified *Shi et al.* [2005] method can be used for all these cases as long as the time interval for averaging the gradient matrix is sufficiently large around the region of peak gradient. We need to note one complication. Note that the blue curve in Figure 5c does not extend past values of $\Delta t_{range}/\Delta t_{half}$ = 4. For greater values, the minimum gradient direction is not clearly steady in any time interval, and in that case the results will depend heavily on the time interval used.

[40] We found that one needs to examine carefully the effect of different values of $\Delta t_{range}/\Delta t_{half}$, especially for the kinetic simulation. To do this we used the fact that we knew the right answer. In order to test again how we would do in a truly blind test, we generated a totally new set of data from the simulation used for Run 3. In this case, the spacecraft trajectory was at an angle of 45° to the current sheet passing 10 c/ω_{pi} downstream of the X point. The coordinates were then rotated using random Euler angles that were unknown to us. We then chose a time interval during which the three directions were relatively constant, and found the maximum, intermediate, and minimum gradient directions for different values of $\Delta t_{range}/\Delta t_{half}$. We looked for convergence of the directions. The directions for $\Delta t_{range}/\Delta t_{half}$ = 8 were within 0.1° of the directions using $\Delta t_{range}/\Delta t_{half}$ = 32, while the directions for $\Delta t_{range}/\Delta t_{half}$ = 4 varied by about 5° from those using $\Delta t_{range}/\Delta t_{half}$ = 32. Based on this, the directions were determined using $\Delta t_{range}/\Delta t_{half}$ = 8. After rotating the resulting directions back to the original coordinate system, the directions for maximum, intermediate, and minimum gradient direction were found to be 9.6°, 9.7°, and 1.5° off from the correct directions. These results were obtained using the modified *Shi et al.* [2005] method from the perturbed gradient. We also calculated the maximum gradient direction using the unmodified method (without subtracting the average gradient). In that case, we found the maximum gradient off by only 0.9° from the correct direction.

[41] Figure 15 shows the median error for 10 trials of Run 3 with different random calibration errors of varying magnitude and different noise errors of the same magnitude (0.01 nT) for the maximum gradient direction $\boldsymbol{e}_{G-max}$ (black curve) and minimum gradient direction $\boldsymbol{e}_{G-min}$ (blue curve) versus the ratio of the calibration error dB_{cal} to the reconnection magnetic field B_{rec} expressed as a percentage. For each trial, a random distribution of dB was assumed for each component of the magnetic field. The horizontal axis shows

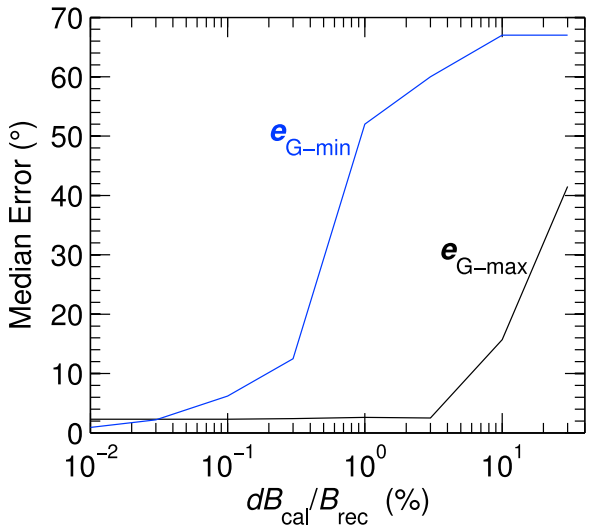

Figure 15. Median error for 10 trials with different random calibration of differing amplitude and noise errors of the same amplitude for the maximum gradient direction $\boldsymbol{e}_{G-max}$ (black curve) and minimum gradient direction $\boldsymbol{e}_{G-min}$ (blue curve) versus the calibration error dB_{cal}. This error is expressed as a percentage of the reconnection magnetic field B_{rec}.

the root mean squared value dB_{cal} for each component of the assumed distribution. Based on Figure 15, the unmodified *Shi et al.* [2005] method can determine the maximum gradient direction to within 3° for calibration errors as large as 3% of the reconnection magnetic field, while in order to find the minimum gradient direction to the same accuracy, the calibration errors must be no larger than 0.03% of the reconnection magnetic field. For reference, the calibration errors assumed here are 0.7% of the reconnection magnetic field.

[42] Based on these numbers, it's likely that the unmodified method can be used to determine the maximum gradient direction, but that the modified method must be used to determine the minimum gradient direction. The results described above for the blind test suggest that the maximum gradient direction might be determined more accurately by the unmodified method. The method is also less complex, not depending on a choice of time interval for averaging the gradient matrix. Combining the maximum gradient direction from the unmodified method with the minimum gradient direction from the modified method, all three angles would be determined within a couple degrees. Another possibility would be to combine the maximum gradient direction from the unmodified method with the maximum variance direction for the magnetic field (yielding the intermediate gradient direction), and from those two directions get the minimum gradient direction.

[43] It should be kept in mind when using the modified *Shi et al.* [2005, 2006] method that subtraction of the gradient $\langle \mathbf{M}^{\nabla B} \rangle_0$ averaged over the interval Δt_{range} (in order to cancel out the effect of constant (in time) calibration errors) results in loss of real information about the average gradient of the real field. In a situation with constant (in time) gradients, the modification would not be likely to give satisfactory results. Comparison between results from the unmodified *Shi et al.* [2005, 2006] methods and the modified methods using the perturbed gradient and time derivative of B may give information on the degree to which calibration errors contaminate the gradients. Ideally, a way will be found to reduce the calibration errors sufficiently as mentioned in Section 2 so that the unmodified and modified methods using the perturbed fields yield the same results. But our estimates indicate that if these calibrations are not reduced, results from the unmodified method may not be satisfactory, especially for the minimum gradient direction (Figure 15).

[44] The effects of explicit time dependence still need to be investigated. It's likely that explicit time dependence will make the procedures we have demonstrated here more difficult. Directions and velocities may be changing with respect to time, in which case they will have to be determined within smaller time intervals. In that case, we would not be able to use extremely large values of $\Delta t_{range}/\Delta t_{half}$. Presumably, as $\Delta t_{range}/\Delta t_{half}$ is increased, the directions would converge toward some values, and then diverge as the timescale over which the data is collected becomes large. Also, large amplitude time-dependent effects in a 3-D kinetic system, associated with physical effects such as waves or nonuniformities in the inflow to the reconnection site, may be larger than what we have in our simulations, and these could have an adverse effect on our ability to obtain accurate information from the *Shi et al.* [2005, 2006] methods and their extension to perturbed fields [*Denton et al.*, 2010].

[45] **Acknowledgments.** RED was supported primarily by NASA grant NNX08AV81G (MMS Theory Program), and to a lesser extent by NSF grant ATM-0120950 (Center for Integrated Space Weather Modeling, CISM, funded by the NSF Science and Technology Centers Programs). JB acknowledges NASA support through the MMS and Solar-Heliophysics Theory programs.

[46] Masaki Fujimoto thanks the reviewers for their assistance in evaluating the paper.

References

Balogh, A., et al. (1997), The Cluster magnetic field investigation, *Space Sci. Rev.*, *79*(1-2), 65–91, doi:10.1023/a:1004970907748.

Birn, J., and M. Hesse (2009), Reconnection in substorms and solar flares: Analogies and differences, *Ann. Geophys.*, *27*, 1067–1078.

Denton, R. E., B. U. Ö. Sonnerup, J. Birn, W. L. Teh, J. F. Drake, M. Swisdak, M. Hesse, and W. Baumjohann (2010), Test of methods to infer the magnetic reconnection geometry from spacecraft data, *J. Geophys. Res.*, *115*, A10242, doi:10.1029/2010JA015420.

Drake, J. F., M. Swisdak, T. D. Phan, P. A. Cassak, M. A. Shay, S. T. Lepri, R. P. Lin, E. Quataert, and T. H. Zurbuchen (2009), Ion heating resulting from pickup in magnetic reconnection exhausts, *J. Geophys. Res.*, *114*, A05111, doi:10.1029/2008JA013701.

Georgescu, E., et al. (2006), Use of EDI time-of-flight data for FGM calibration check on Cluster, in *Proceedings of the Cluster and Double Star Symposium: 5th Anniversary of Cluster in Space*, *Eur. Space Agency Spec. Publ.*, *ESA SP-598*, 1–7.

Mozer, F. S., and A. Retinò (2007), Quantitative estimates of magnetic field reconnection properties from electric and magnetic field measurements, *J. Geophys. Res.*, *112*, A10206, doi:10.1029/2007JA012406.

Shay, M. A., J. F. Drake, and M. Swisdak (2007), Two-scale structure of the electron dissipation region during collisionless magnetic reconnection, *Phys. Rev. Lett.*, *99*(15), 155002, doi:10.1103/PhysRevLett.99.155002.

Shen, C., X. Li, M. Dunlop, Z. X. Liu, A. Balogh, D. N. Baker, M. Hapgood, and X. Wang (2003), Analyses on the geometrical structure of magnetic field in the current sheet based on cluster measurements, *J. Geophys. Res.*, *108*(A5), 1168, doi:10.1029/2002JA009612.

Shen, C., X. Li, M. Dunlop, Q. Q. Shi, Z. X. Liu, E. Lucek, and Z. Q. Chen (2007a), Magnetic field rotation analysis and the applications, *J. Geophys. Res.*, *112*, A06211, doi:10.1029/2005JA011584.

Shen, C., M. Dunlop, X. Li, Z. X. Liu, A. Balogh, T. L. Zhang, C. M. Carr, Q. Q. Shi, and Z. Q. Chen (2007b), New approach for determining the normal of the bow shock based on Cluster four-point magnetic field measurements, *J. Geophys. Res.*, *112*, A03201, doi:10.1029/2006JA011699.

Shi, Q. Q., C. Shen, Z. Y. Pu, M. W. Dunlop, Q. G. Zong, H. Zhang, C. J. Xiao, Z. X. Liu, and A. Balogh (2005), Dimensional analysis of observed structures using multipoint magnetic field measurements: Application to Cluster, *Geophys. Res. Lett.*, *32*, L12105, doi:10.1029/2005GL022454.

Shi, Q. Q., C. Shen, M. W. Dunlop, Z. Y. Pu, Q. G. Zong, Z. X. Liu, E. Lucek, and A. Balogh (2006), Motion of observed structures calculated from multi-point magnetic field measurements: Application to Cluster, *Geophys. Res. Lett.*, *33*, L08109, doi:10.1029/2005GL025073.

Shi, Q. Q., et al. (2009a), Spatial structures of magnetic depression in the Earth's high-altitude cusp: Cluster multipoint observations, *J. Geophys. Res.*, *114*, A10202, doi:10.1029/2009JA014283.

Shi, Q. Q., et al. (2009b), Cluster observations of the entry layer equatorward of the cusp under northward interplanetary magnetic field, *J. Geophys. Res.*, *114*, A12219, doi:10.1029/2009JA014475.

Sonnerup, B. U. Ö., S. Haaland, G. Paschmann, M. W. Dunlop, H. Reme, and A. Balogh (2006), Orientation and motion of a plasma discontinuity from single-spacecraft measurements: Generic residue analysis of Cluster data, *J. Geophys. Res.*, *111*, A05203, doi:10.1029/2005JA011538.